AGU PUBLICATIONS

JGR

Journal of Geophysical Research: Space Physics

RESEARCH ARTICLE
10.1002/2016JA022445

Key Points:
- MHD simulation of impulses during substorms
- It takes approximately 70 s for waves to travel from the midtail to the aurora region
- MHD waves travel faster through the lobes, and they reach higher latitudes earlier than lower latitudes

Supporting Information:
- Supporting Information S1
- Movie S1

Correspondence to:
B. Ferdousi,
bhr9@wildcats.unh.edu

Citation:
Ferdousi, B., and J. Raeder (2016), Signal propagation time from the magnetotail to the ionosphere: OpenGGCM simulation, *J. Geophys. Res. Space Physics*, *121*, doi:10.1002/2016JA022445.

Received 27 JAN 2016
Accepted 5 JUL 2016
Accepted article online 12 JUL 2016

Signal propagation time from the magnetotail to the ionosphere: OpenGGCM simulation

Banafsheh Ferdousi[1] and Joachim Raeder[1]

[1] Department of Physics and EOS Space Science Center, University of New Hampshire, Durham, New Hampshire, USA

Abstract Distinguishing the processes that occur during the first 2 min of a substorm depends critically on the correct timing of different signals between the plasma sheet and the ionosphere. To investigate signal propagation paths and signal travel times, we use a magnetohydrodynamic global simulation model of the Earth magnetosphere and ionosphere, OpenGGCM-CTIM model. By creating single impulse or sinusoidal pulsations in various locations in the magnetotail, the waves are launched, and we investigate the paths taken by the waves and the time that different waves take to reach the ionosphere. We find that it takes approximately about 27, 36, 45, 60, and 72 s for waves to travel from the tail plasma sheet at $x = -10, -15, -20, -25$, and $-30\ R_E$, respectively, to the ionosphere, contrary to previous reports. We also find that waves originating in the plasma sheet generally travel faster through the lobes than through the plasma sheet.

1. Introduction

The nightside of the magnetosphere is a very dynamic region, where substorms can release a substantial amount of energy in an explosive fashion. Even though many physical models explaining the substorm process have been proposed, the onset mechanism of substorms is still an unsolved problem in the field of space physics. The phenomena associated with substorms happen so fast that it is difficult to establish the causal relation between the disturbances. There are several models suggesting a specific trigger of substorms, and some of the most promising ones include the current disruption model (CD) proposed by *Lui* [1996] and *Lui* [2004], the ballooning model by *Roux et al.* [1991], the near-Earth natural line (NENL) model by *Russell and McPherron* [1973], *Hones* [1984], and *Baker et al.* [1996], and the plasma intrusion into the polar cap model, recently proposed by *Nishimura et al.* [2010] and *Lyons et al.* [2010].

The first two models suggest that triggering occurs close to the Earth (~ -8 to $-10\ R_E$) by the current disruption or the ballooning instability, and the NENL model predicts that reconnection in the midtail (~ -15 to $-30\ R_E$) triggers the substorm. Even though the Time History of Events and Macroscale Interactions during Substorms (THEMIS) mission was specifically designed to resolve the controversy between the NENL and the CD models, the observations are still divided between these two models. One of the main criticism of the NENL model observed by THEMIS is to the time delay between the reconnection onset and the substorm ground signatures. *Angelopoulos et al.* [2008] reported that it takes ~96 s for disturbances to propagate from $x \sim -20\ R_E$ to aurora break up and 117 s to high latitude Pi2 pulsations. In the other study, *Gabrielse et al.* [2009] concluded that disturbances travel ~ 64 and 89 s from $x \sim -15.7\ R_E$ to the auroral intensification and Pi2 pulsations, respectively. Since waves cannot travel that fast in the magnetotail according to previous magnetohydrodynamic (MHD) wave travel time studies, those results were disputed by *Lui* [2009].

Also, *Nishimura et al.* [2010] based on statistical analysis of THEMIS all-sky imager data suggested that there is a repeatable sequence of events which leads to a substorm onset: a poleward boundary intensification is followed by the emergence of a north-south arc (an auroral streamer), moving equatorward, and leading to the substorm onset.

Distinguishing the phenomena associated with substorms is difficult to achieve with data alone since signals are sometimes ambiguous, or they may not be observed in the right locations. Therefore, it is important to develop a realistic model of magnetohydrodynamic (MHD) wave propagation speeds associated with disturbances in order to establish the causal relation between the events. Both the auroral brightening and Pi2 pulsations are markers of substorm expansion phase onset; however, Pi2 pulsations are easier to observe than

auroral signatures. Because Pi2 pulsations generally precede the onset of auroral brightening [*Liou et al.*, 2000], Pi2 pulsations provide a convenient lower limit of the time for energy to reach the ionosphere from the tail, provided that the MHD travel times are known with sufficient accuracy.

There are a couple of studies that focus on MHD wave travel time in the magnetosphere [e.g. *Lin et al.*, 2009; *Chi et al.*, 2009]. The *Lin et al.* [2009] study assumes that the MHD wave propagate along the magnetic field lines in the tail plasma sheet until $x = -10\ R_E$ with magnetosonic wave speed. They then propagate along the dipole magnetic field lines at the Alfvén velocity after $-10\ R_E$ to the Earth. In order to determine the Alfvén and magnetosonic velocities in the magnetotail, *Lin et al.* [2009] used empirical models of density, temperature, and magnetic field along the path. In the *Chi et al.* [2009] study, the Tsyganenko 89 magnetosphere model [*Tsyganenko*, 1989], plasma density, and temperature data were used to calculate the magnetosonic and the Alfvén velocities for a wide range of latitudes.

In this paper, we use the OpenGGCM numerical global simulation model to study MHD wave propagation paths in the magnetotail and their travel times to reach the ionosphere. The waves are launched by perturbing the plasma pressure in various locations in the plasma sheet. Their travel times are determined based on their arrival time signatures in the ionosphere.

The outline of the rest of paper is as follows. Section 2 focuses on the OpenGGCM model description and the methodology. In section 3, we present our result describing the MHD wave propagation paths in the magnetotail and their ionosphere signatures. Finally, we discuss our results in the context of previous studies and observations in section 4.

2. Simulation

2.1. OpenGGCM-CTIM Model

OpenGGCM is a numerical global model solving MHD equations in the Earth magnetosphere outside of 3 R_E. The Coupled Thermosphere Ionosphere Model (CTIM) [*Fuller-Rowell et al.*, 1996] is then coupled from 3 R_E to the Earth to the OpenGGCM model [*Raeder et al.*, 2009].

The magnetosphere extends from 20 R_E in sunward direction to several hundred R_E in antisunward direction, and to 48 R_E in y/z direction. The grid style is in a stretched Cartesian coordinate with resolution varying from 0.1 to 0.2 R_E in magnetopause, and 0.1 to 0.3 R_E in the near-Earth tail. The model can either be driven by real solar wind data (velocity, magnetic field, density, and pressure) from solar wind monitor satellites like ACE or WIND, or it can be used with generic solar wind conditions.

The inner magnetosphere is coupled via the closure of field-aligned current (FAC) to the ionosphere. The ionosphere solves potential equation on a sphere, yielding the ionospheric convection potential [*Fedder and Lyon*, 1987], which maps back to the inner magnetosphere as the boundary conditions. The ionosphere extends from 58° to 90° magnetic latitudes since mapping originates from 3 R_E. The more detailed description of OpenGGCM model can be found at *Raeder* [2003] and *Raeder et al.* [2009], so we refer our readers to those papers. The OpenGGCM model is capable of generating many magnetosphere phenomenon including substorms [*Raeder et al.*, 2001a; *Ge et al.*, 2011; *Gilson et al.*, 2012; *Raeder et al.*, 2013], ballooning modes [*Zhu et al.*, 2009; *Raeder et al.*, 2010], storms [*Raeder et al.*, 2001b], interplanetary shocks [*Oliveira and Raeder*, 2014], flux transfer events [*Raeder*, 2006], dayside reconnection [*Connor et al.*, 2014, 2015], and cusp dynamics [*Connor et al.*, 2012].

2.2. Methodology

The simulation uses the geocentric solar ecliptic coordinate system. The numerical box extends from 21 R_E in the sunward direction to 500 R_E down the tail. The box size in y/z direction (perpendicular to Sun-Earth line) extends from −48 to 48 R_E. There is a total of 16×10^6 grid cells in this simulation, with the highest resolution close to the plasma sheet with the minimum grid cell size of 0.1 R_E.

To study waves propagation from the tail to the ionosphere, waves are generated by an impulse or by a sinusoidal pulsations at different locations in the plasma sheet within the OpenGGCM model. The impulse is created by perturbing plasma pressure at a single point with a delta function, or sinusoidal pulsations are created by $P \sim \sin(2\pi/T)$ function, where T is the period of the wave. The increase in pressure is strong enough to launch linear waves that can be followed through the system, but not as strong as to create nonlinear perturbations. The impulses are mainly generated to study the wave travel time in the magnetotail, to evaluate the

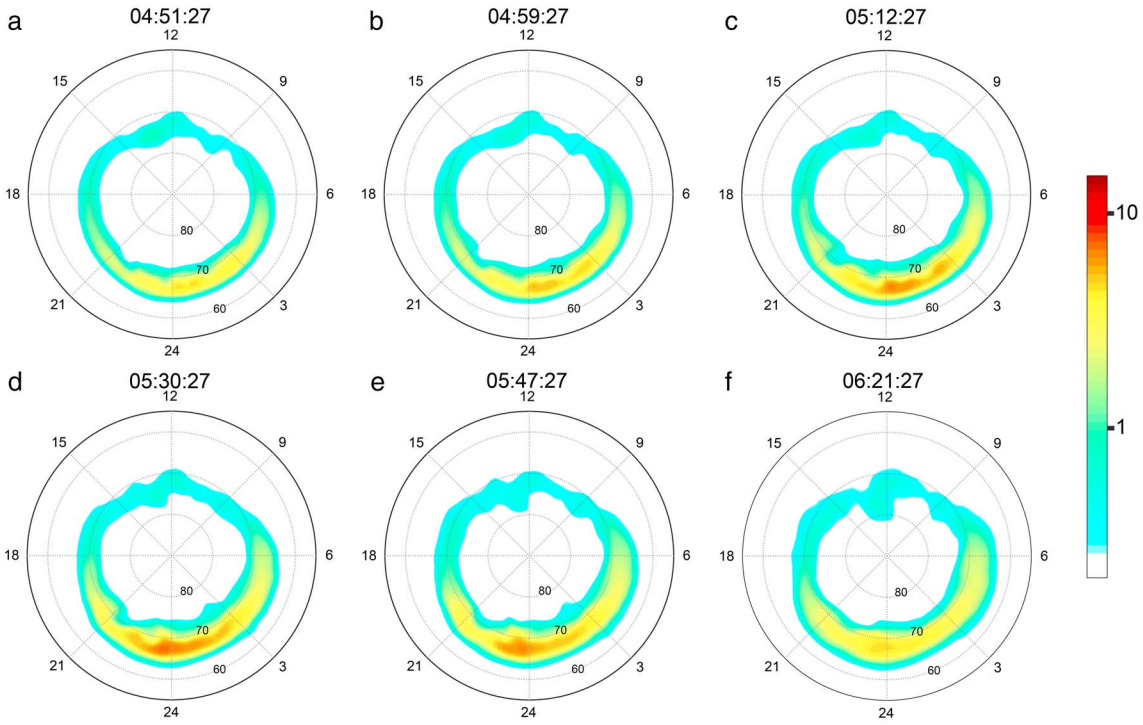

Figure 1. Diffuse auroral electron precipitation energy flux in mW/m^2. The substorm starts at 4:51:27 UT. The westward surge starts at 4:59:27. The expansion continues until it reaches the maximum at 5:30:27 UT. Then the substorm dims and it ceases at 6:21:57 UT.

characteristics of the signals, and to determine the latitude and longitude of wave arrival in the ionosphere. The sinusoidal pulsations on the other hand are better suited to visualize the wave propagation paths and to distinguish different MHD wave modes.

Since waves are partially reflected at gradients, because their energy spreads out more quickly in regions of high phase velocity, and because of geometric attenuation, the amplitude of the waves can become very low. In order to visualize such waves, two simulation runs, one with the perturbation and the other without it, are subtracted from each other. Even though this method eliminated most of the perturbations not related to the wave, there is still some numerical noise closer to the Earth. The numerical noise is removed by using a spatial Gaussian filter in a box extending from $x = (-10, 15)$ and $z = (-10, 10)\, R_E$ with the cutoff frequency of 0.053 Hz. We used the same approach to improve the visualization of signals in the ionosphere, where we plot the ΔFAC and the north-south component of ground magnetic field perturbation (ΔB_θ) to determine signal arrival times and locations.

We use solar wind data for substorm event of 26 February 2008, as reported by *Angelopoulos et al.* [2008], in which the auroral signature of substorm onset (auroral intensification) was reported to occur at 4:51:39 UT. Our model is able to produce the same substorm event but at an earlier time. Even though the OpenGGCM model does not produce auroral emission, it produces the energy flux and mean energy of two populations of precipitating electrons. The former population corresponds to the thermal electron flux from the inner magnetosphere forming the diffuse aurora, and the latter is the result of electrons that have been accelerated in regions of upward FAC forming discrete aurora [*Raeder et al.*, 2009]. In this paper, we use the modeled diffuse aurora to identify the auroral onset because it is more comparable to real data substorm observations.

Figure 1 shows diffuse aurora precipitation in mW/m^2 in Northern Hemisphere at six different times. At 4:51:27 UT, the first indication of substorm onset is visible around midnight and 68° magnetic latitudes (Figure 1a). Using more detailed plots, we find the intensification already started at 4:45 UT which is 6 min prior to the onset that was observed from data. The time difference between real data observation of substorm onset and MHD simulation of the event could be due to the location of solar wind monitor, which creates uncertainty in the transit time from the monitor to the Earth. The aurora expands northward and westward between 4:59:27 and 5:12:27 UT (Figures 1b and 1c). The aurora reaches its maximum intensification

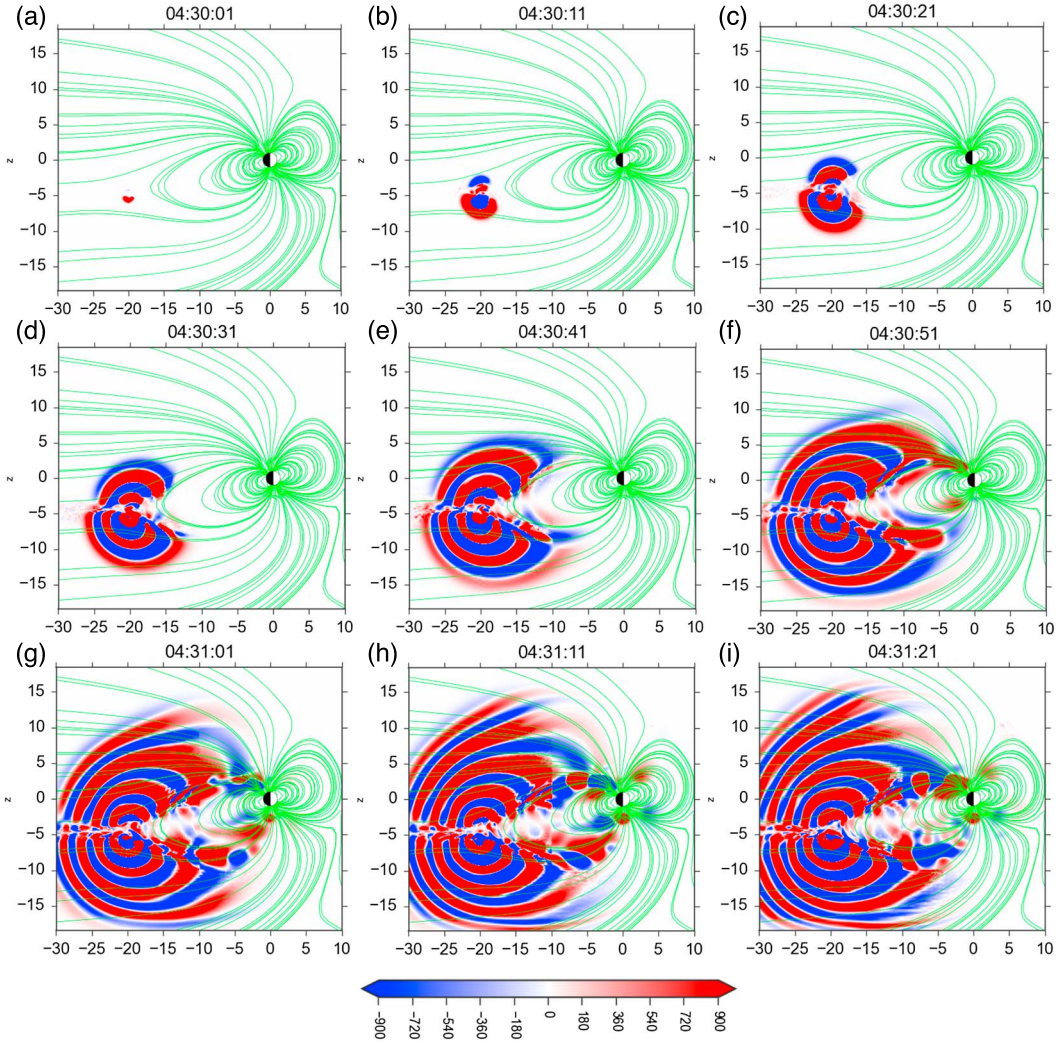

Figure 2. The difference in Poynting flux (ΔS_z) in μW/m^2 in the meridian plane. The sinusoidal pulsation is created at $x = -20\ R_E$ with period of $T = 12$ s in the plasma sheet before the reconnection onset during a real substorm event.

at 5:30:27 UT (Figure 1d). Later the auroral intensification begins to dim at 5:47:27 UT, and it ceases around 6:21:27 UT (Figures 1e and 1f, respectively).

It is complicated to find the exact timing of reconnection onset in the simulation because the tail is very dynamic during the substorm. Since the disturbances are spatially localized in the dawn-dusk direction, any specific observed disturbance might not exactly mark the beginning of a reconnection. Therefore, we create both impulses and sinusoidal pulsations during the late substorm growth phase when the plasma sheet has thinned and just before the expected reconnection onset and the development of fast earthward flows. The impulses and sinusoidal pulsations are launched at 4:30 UT in the center of plasma sheet at x = −10, −15, −20, −25, and −30 R_E.

3. Results

3.1. Wave Paths in the Magnetotail

Figure 2 shows the time evolution of the Poynting flux (ΔS_z) in μW/m^2 indicating the wave energy flow direction. Because the plots are created by subtracting two simulation runs from each other, the background magnetic and electric fields are removed, and Poynting flux is based on perturbation in magnetic and electric field $\mathbf{S} = 1/\mu_0(\delta\mathbf{E} \times \delta\mathbf{B})$, in which the electric field is calculated via frozen in condition $\mathbf{E} = -\mathbf{V} \times \mathbf{B}$.

In this figure, the waves are generated by sinusoidal pulsation ($P = 200 \sin(2\pi/T)$) in pPa with period of $T = 12$ s at $x = -20\ R_E$ during the real substorm event on 26 February 2008 [*Angelopoulos et al.*, 2008] at 04:30 UT.

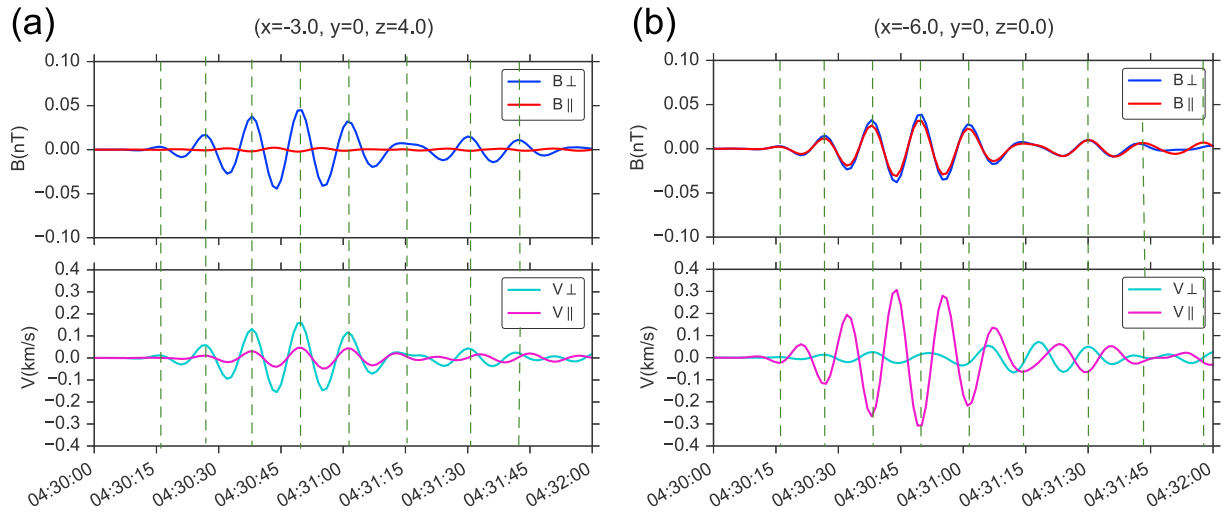

Figure 3. Time series of the parallel and perpendicular components of velocity and magnetic field in the lobe and plasma sheet near the Earth. The waves are generated by sinusoidal pulsation at $x = -20\,R_E$ with period of $T = 12$ s. Data are band-pass filtered from 0.071 to 0.1 Hz.

There is a 10 s time interval between each plot. In addition, a supporting information Movie S1 with the resolution of 1 s is provided. We choose the 12 s period to better visualize wave fronts, since the typical Pi2 pulsations period is comparable to the propagation time of the wave and thus does not show wave fronts well.

As Figure 2 shows, the wave fronts first travel isotropically in all directions, but the fronts that are propagating toward the lobes travel faster than the ones propagating through the plasma sheet and therefore the oval shape in Figure 2b forms. Because the magnetic field increases near the Earth, the wave amplitude decreases; thus, it is more difficult to see the wave fronts in the lobe near the Earth in Figure 2e. Meanwhile, other wave fronts continue to propagate through plasma sheet until they reach the Earth closed field line region, where they continue to travel along the magnetic field lines (Figures 2d to 2i).

We also performed time series analysis at different points in the magnetotail in order to obtain the wave modes along their paths. Before discussing the details of the time series results, we briefly review some characteristics of MHD waves, in particular the difference between the fast and the Alfvén mode. Based on the dispersion relation of MHD waves in cold plasma, shear Alfvén waves only travel along magnetic field. Alfvén wave propagation sets plasma into the perpendicular motion to the propagation vector k and background field [*Kivelson and Russell*, 1995]; thus, one expects perturbations in $B_\perp$ and $V_\perp$. Based on the relation $B_\perp \sim \pm V_\perp$, the magnetic field and velocity are either in phase, i.e., the wave travels in the opposite direction relative to the background field, or they are in antiphase, i.e., the wave travels in the same direction of the background field [*Priest*, 2012]. The fast or compressional Alfvén wave mode can propagate in all directions, and it has perturbations in both the parallel and the perpendicular components of the magnetic field. Also, there is correlation or anticorrelation between $B_\perp$ and $V_\parallel$, which are either in phase or antiphase relative to each other, when the wave vector has a component parallel to the background field.

Figure 3 is the time series of parallel and perpendicular components of the magnetic field perturbation ($B_\parallel$ in red and $B_\perp$ in blue) and the parallel and perpendicular plasma velocity perturbation ($V_\parallel$ in magenta and $V_\perp$ in cyan) in the lobe and plasma sheet near the Earth. We calculated the parallel component via $B_\parallel = \hat{b} \cdot \delta\vec{B}$ relation, where $\hat{b}$ is a unit vector tangential to the background magnetic field, and $\delta\vec{B}$ is the perturbation in the magnetic field. For the perpendicular component, we used $\vec{B}_\perp = \delta\vec{B} - \vec{B}_\parallel$, and the same relations were used to calculate $\vec{V}_\parallel$ and $\vec{V}_\perp$. Since our source wave has a period of 12 s, we band-pass filtered our data from 0.071 to 0.1 Hz corresponding to a period of 14 to 10 s, respectively.

The Figure 3a (top) displays $B_\parallel$ and $B_\perp$, where there is perturbation in $B_\perp$ and no perturbation in $B_\parallel$. In Figure 3a (bottom), there is perturbation in $V_\perp$, which is in phase with $B_\perp$ in the lobe near the Earth ($x = -3.0, y = 0.0$, and $z = 4$ R_E). Based on the MHD wave properties described above, we identify this wave as an Alfvén mode. Figure 3b shows time series taken in the plasma sheet ($x = -6.0, y = 0.0$, and $z = 0$ R_E) near the Earth, in which there are perturbations in both parallel and perpendicular components of magnetic field with the same amplitude, and $B_\perp$ and $V_\parallel$ are in phase, which is consistent with a fast mode wave.

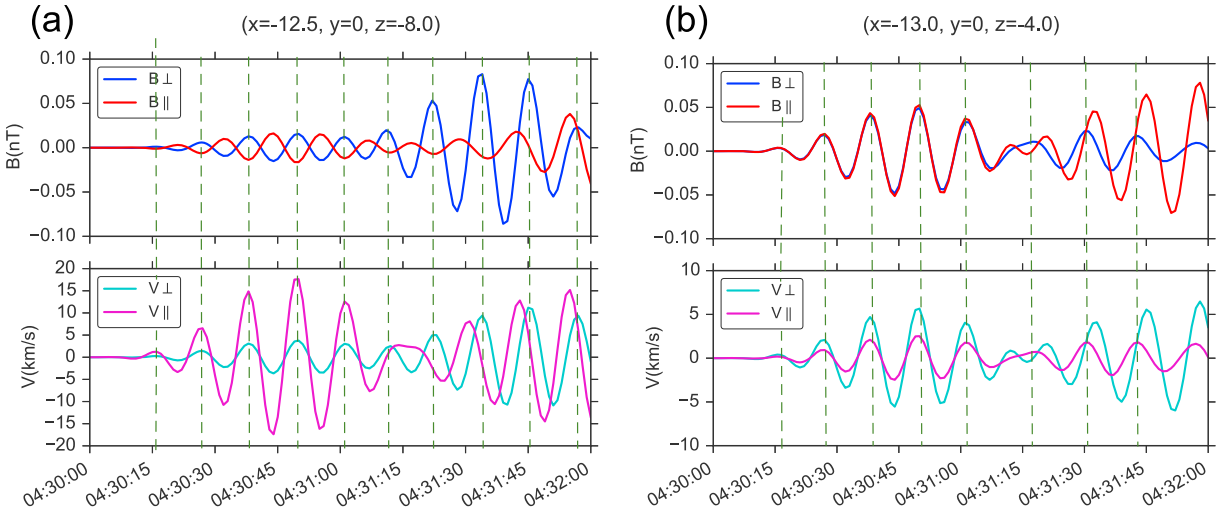

Figure 4. Time series of the parallel and perpendicular components of velocity and magnetic field in the PSBL and plasma sheet in the midtail region. The waves are generated by sinusoidal pulsation at $x = -20\ R_E$ with period of $T = 12$ s. Data are band-pass filtered from 0.071 to 0.1 Hz.

In Figure 4a ($x = -12.5$, $y = 0.0$, and $z = -8.0$), there are perturbation in all components of magnetic field and velocity, and $B_\perp$ and $V_\perp$ are in phase until 4:31:15 UT. At this time, the amplitude of perturbation in $B_\perp$ increases compared to $B_\parallel$. We interpret the first part of wave as a fast mode, while an Alfvén wave propagating along different path arrives at the same location around 65 s later. Figure 4b shows time series in the plasma sheet at $x = -14.0$, $y = 0.0$, and $z = -4.0\ R_E$, where there are perturbations in $B_\parallel$ and $B_\perp$ with almost the same amplitude, and perturbations in $B_\perp$ and $V_\parallel$ that are in phase, which is consistent with a fast mode wave.

We can now develop an overall picture of wave propagation in the magnetotail based on time series analysis (Figures 3 and 4) and wave flow energy direction (Figure 2). The wave fronts first propagate isotropically in all directions as fast mode. The waves then take two different paths. One type travels magnetosonically through the plasma sheet until the wave front reaches the dipolar field near the Earth; it then interacts with the dipole magnetic field and continues to propagate along the dipolar field lines as an Alfvén mode into the ionosphere. In the other path, the wave travels magnetosonically through the lobes where it converts to an Alfvénic mode as it reaches near the Earth. The similar but more simpler wave path was suggested by *Tamao* [1964], such that

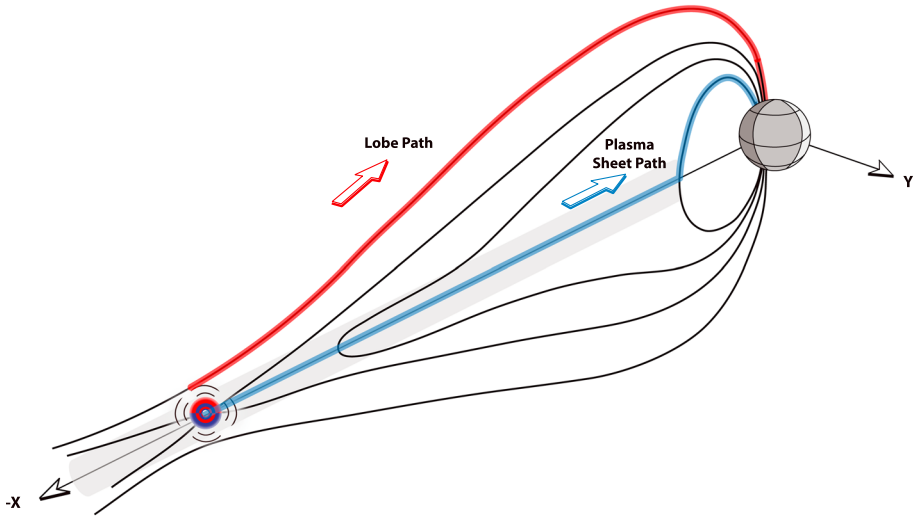

Figure 5. Schematic of possible wave path in the magnetotail. The blue line is the plasma sheet path in which wave travels through the plasma sheet as fast mode until it reaches the dipolar field where converts to Alfvénic mode and continues along field lines. In the lobe path (red line) the wave travels through the lobes as magnetosonic until it reaches high magnetic field or gradient in density where it converts to the Alfvénic mode.

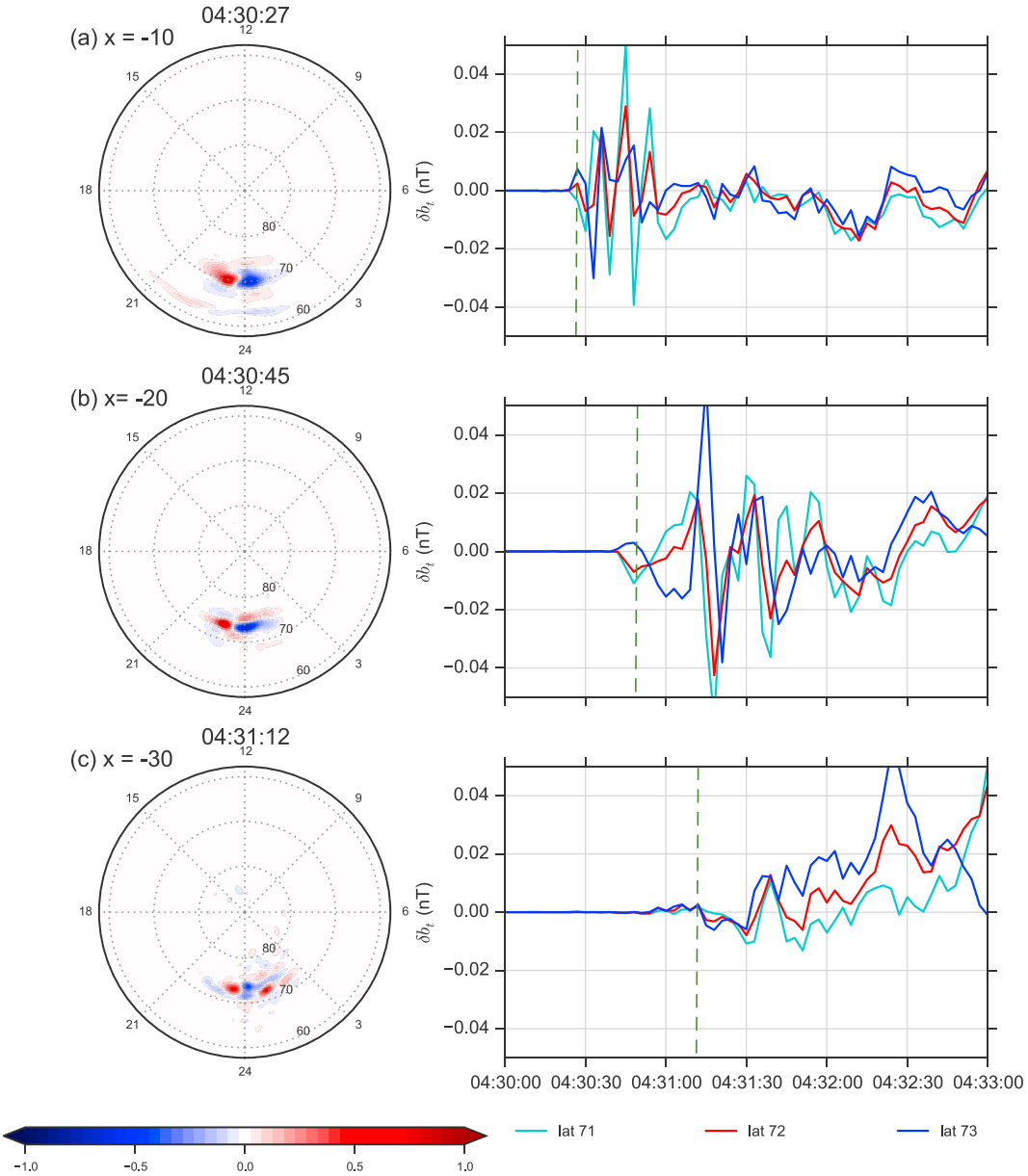

Figure 6. (a–c) The ionospheric arrival impulses generated at different locations in the magnetotail: $x = -10, -20$, and -30 R_E, respectively. Figure 6 (left column) is ΔFAC (μA/m^2) in the Northern Hemisphere polar cap. The dashed circles indicate magnetic latitude with 10° increment. Figure 6 (right column) is ΔB_θ at midnight and different magnetic latitudes (71° to 73°).

the fast mode wave generates an Alfvén mode wave, which then transmits wave energy to the ionosphere. *Tamao* [1964] also suggested that the maximum wave energy was transferred when the wave propagated along the so-called, "Tamao Path." Figure 5 shows a schematic view of these paths in the magnetotail, where the blue line is the plasma sheet path and the red line is the lobe path.

The conversion from the fast mode to the Alfvén mode requires an inhomogeneity in the magnetic field or density. As the waves pass through the plasma sheet boundary layer (PSBL) or near the Earth, they encounter both strong density and field gradients, where the fast compressional mode will covert to the shear Alfvén mode. The fast-Alfvén mode conversion in the PSBL and the magnetic lobes was also observed in Polar satellite data [*Keiling et al.*, 2005] and MHD simulations [*Allan and Wright*, 2000; *Lysak and Song*, 2004; *Lysak et al.*, 2015].

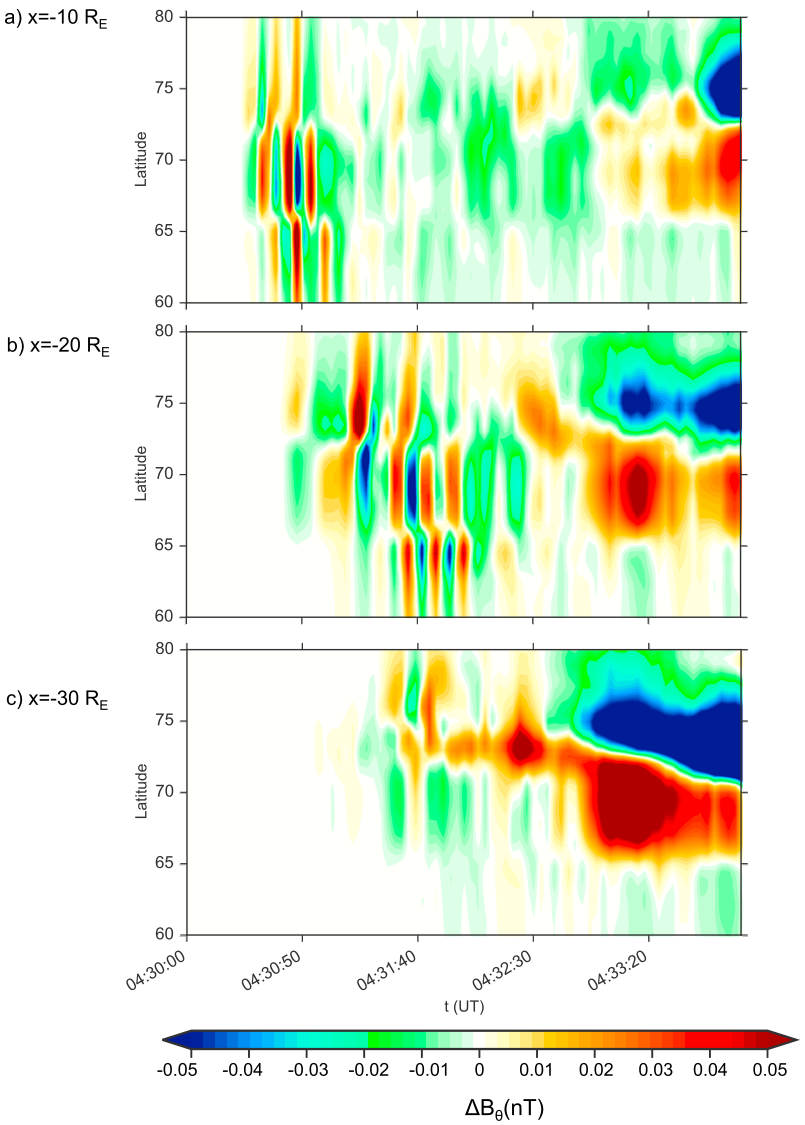

Figure 7. Time histories of ΔB_θ at midnight MLT and as a function of time and latitude. The wave sources are located at (a) $x = -10$, (b) $x = -20$, and (c) $x = -30\,R_E$, respectively. The signals arrive at all latitudes almost simultaneously when the source is located near the Earth, and the signals reach higher latitudes earlier than lower latitudes when the source is located in the midtail.

3.2. Ionosphere Signatures

In order to determine signal arrival time in the ionosphere, we plot time series of difference in the north-south component of magnetic field perturbation ΔB_θ and the difference in field-aligned current (ΔFAC) in the ionosphere. Figures 6a–6c show signal arrival times in the ionosphere for waves originating from −10, −20, and $-30\,R_E$ in the magnetotail, respectively. Note that the waves for these plots are generated by a single impulse (delta function source) and not sinusoidal pulsations. The time series of ΔB_θ is at midnight magnetic local time and different geomagnetic latitudes of the ionosphere ranging from 71° to 73° as shown in Figure 6 (right column).

Signal arrival time is determined at the time of the first peak in the ground magnetic perturbation (ΔB_θ) as the dashed line in Figure 6 indicates. This characteristic is similar to *Chi et al.* [2001], *Chi and Russell* [2005], and *Chi et al.* [2006, 2009] studies.

Depending on the locations of the wave source in the tail, signals arrive at different times in the midnight region of the ionosphere. Figure 7 shows the time development of ground magnetic field (ΔB_θ) at magnetic local time (MLT) = 0 and latitudes ranging from 60° to 80°. For waves source located near the Earth ($x = -10\,R_E$),

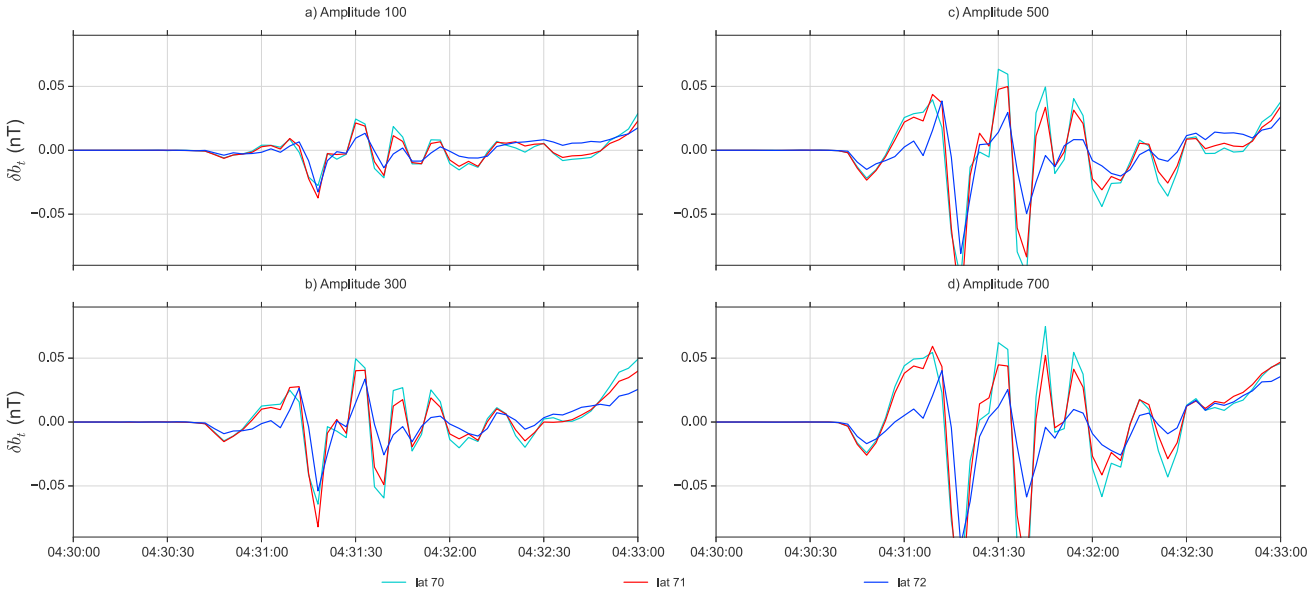

Figure 8. The time series of ΔB_θ at midnight and different magnetic latitudes. All waves are generated by an impulse at $x = -20\,R_E$ with different amplitudes. The wave travel time does not depend on impulse amplitude.

signals reach all magnetic latitudes almost simultaneously. However, when the wave source moves further away from the Earth, the signals arrive at higher latitudes slightly earlier than lower latitudes. When waves originate around $x = -20\,R_E$, signals arrive at higher latitudes (65° to 80°) 20 s earlier than at lower latitudes (60° to 65°). For waves originating at $x = -30\,R_E$, signals first reach magnetic latitudes around 73°. The signals then reach the 65° and higher latitudes around 20 s later and latitudes below 65° around 40 s later.

We also note that the waves are more spread out in local time when the impulses are created closer to the Earth, whereas the signals are more localized for midtail impulses as Figure 6 (left column) shows. This difference is probably the result of the simple mapping of magnetic field lines from the magnetotail to the ionosphere and the nature of the waves that take either the plasma sheet path or the lobe path, respectively. As described in section 3.1, the waves traveling along the plasma sheet path are mostly magnetosonic and travel in all directions azimuthally. However, the waves propagating along the lobes are mostly Alfvénic, with their group speed strictly aligned along field lines, leading to the more localized signatures. Also, as expected, the amplitude of the signal decreases as the impulse is generated further away in the tail as the comparison between time series δB_θ in Figure 6 shows.

In order to examine if there are any effects of wave amplitude, we changed the amplitude of the plasma pressure of impulses to vary between 100, 300, 400, and 500 pPa in the magnetotail at fixed locations and find that the signal arrival time does not depend on amplitude of an impulse as displayed in Figure 8. Thus, the waves are linear, and signal arrival times are independent of the amplitude of waves.

4. Discussion

Figure 9 shows the space-time diagram of MHD wave travel times from the magnetotail to the ionosphere in the OpenGGCM (red solid line), the *Lin et al.* [2009] model (blue solid line), and the *Chi et al.* [2009] model (green solid line), which are plotted along with 11 substorm events (dots) adopted from *Lin et al.* [2009]. The *Lin et al.* [2009] MHD wave travel time is based on the Figure 4 of that paper, and the *Chi et al.* [2009] MHD wave travel time is adopted from Figure 2b of the paper for $L = 10$, which is the minimum travel time in that plot.

The onset time of the 11 substorms were taken at the time of poleward expansion of aurora, and the events were investigated and published previously by different scientists and were collected by *Lin et al.* [2009]. For a more detailed description of these substorms, we refer readers to the *Lin et al.* [2009] paper. The dashed line at $x = 0$ and $\Delta t = 0$ in Figure 9 is the auroral onset time of the 11 substorms and the signal arrival time in the ionosphere in the OpenGGCM model. Data points of the same color and symbol belong to the same substorm event, and substorm events that happen in the same day are shown by number in parentheses according to

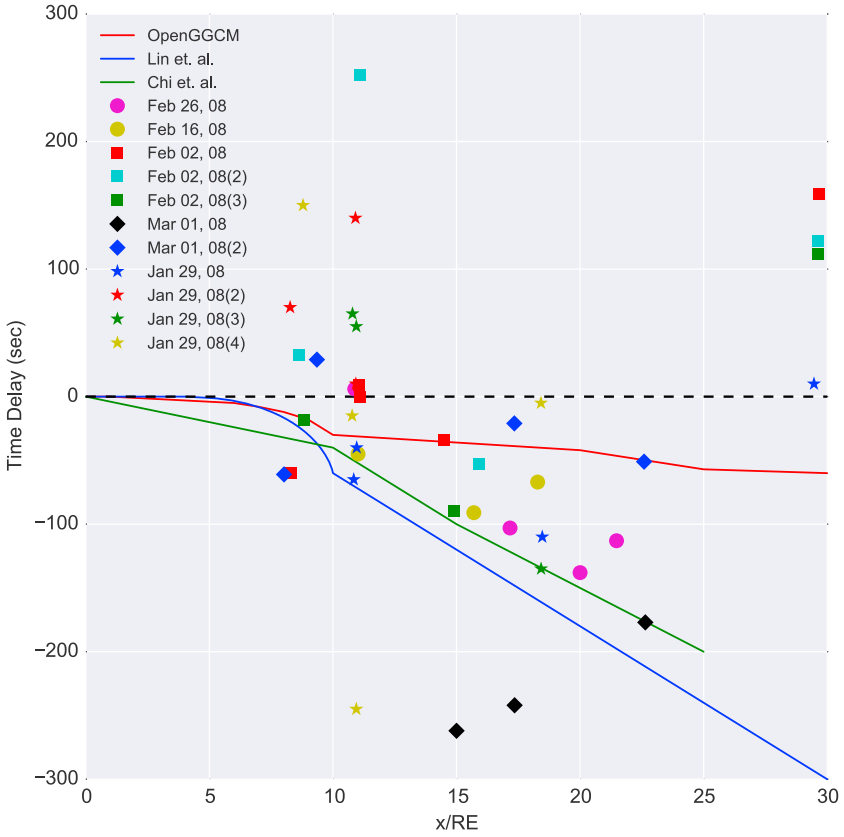

Figure 9. MHD wave travel space-time diagram. The red solid line is the MHD travel time in the OpenGGCM model. The blue and green solid lines are MHD wave travel times published by *Lin et al.* [2009] and *Chi et al.* [2009], respectively. The data points indicate 11 substorm events adapted from Table 1 of *Lin et al.* [2009]. The same symbol and color data points belong to the same substorm event, and the events happened in the same day are numbered in parenthesis [*Lin et al.*, 2009].

Table 1 of *Lin et al.* [2009]. Data points below the dashed line ($\Delta t < 0$) are substorm signatures before the auroral onset, and the ones above the dashed line ($\Delta t > 0$) are the space signatures of substorms occurring after ground onset of the respective substorm. Of course, ionosphere signatures that occur before the time of space signatures with the MHD travel time added cannot cause the latter.

Figure 9 shows that most of the observed substorm signatures fall below OpenGGCM MHD wave travel time curve and thus can be the cause of observed auroral onsets. Clearly, most of the events would be ruled out by the *Lin et al.* [2009] and *Chi et al.* [2009] models as causing the ground signatures. However, many of the observed time difference between tail signatures and the auroral onset are significantly longer than what our model would predict. For example, our model predicts a travel time of 72 s from 30 R_E to the ionosphere. Therefore, many of reported tail signatures that are compiled in Figure 9 have either no direct causal relation to the auroral onset, or alternatively the observed auroral onset is not the very first ground signatures, i.e., earlier ground signatures have been missed, or OpenGGCM underestimates wave travel time. However, we consider the latter unlikely, because the density and field values in the OpenGGCM compare well to values that are typically observed in the tail.

Our result is significantly different from the previous studies of *Lin et al.* [2009] and *Chi et al.* [2009], who suggested that the waves take much longer to reach the ionosphere (~ 100–300 s). The difference seems to arise from the assumed Alfvén and magnetosonic speeds and wave travel path in those studies. *Lin et al.* [2009] used an empirical model of plasma density, temperature, and magnetic field to approximate the Alfvén and the magnetosonic speeds in the magnetotail. *Chi et al.* [2009] took a similar approach to calculate MHD wave velocities. The magnetic field, plasma density, and temperature based on empirical model used in *Chi et al.* [2009] and *Lin et al.* [2009] are different from the ones based on OpenGGCM model, which leads to different MHD wave velocities. Using an empirical magnetic field model can be challenging since empirical models like

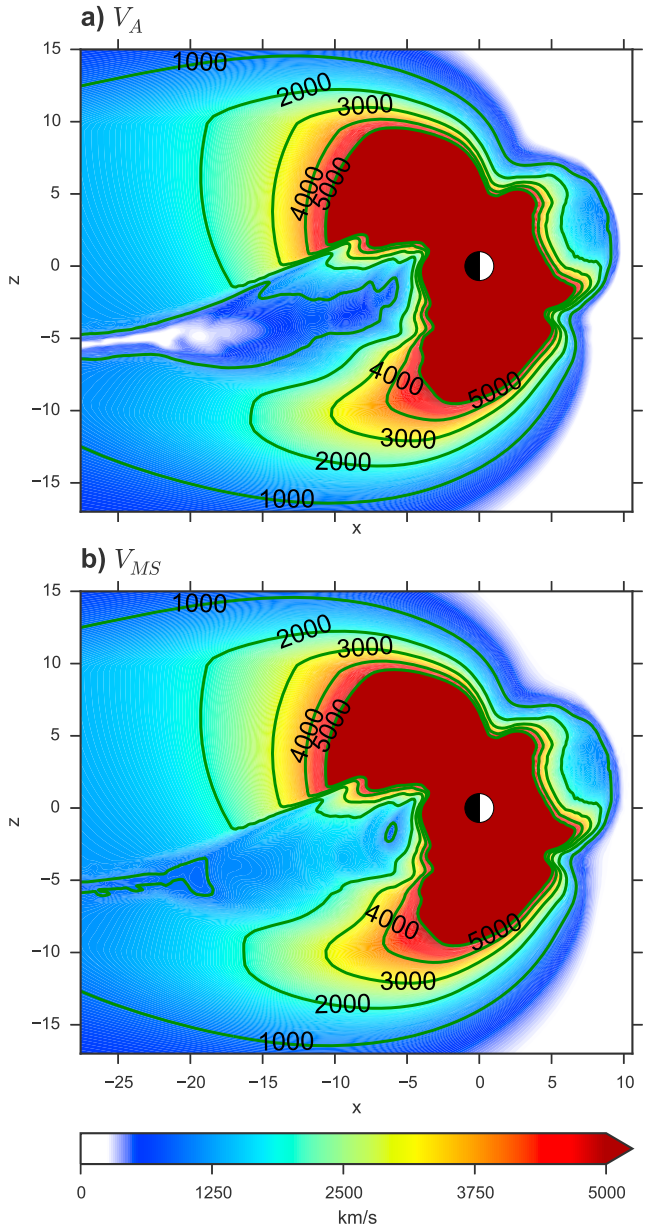

Figure 10. (a) Color coded the Alfvén velocity and (b) the magnetosonic velocity in the meridian plane of the magnetotail. The Alfvén and magnetosonic velocities vary from 1500 to 5000 in the lobes. In the plasma sheet Alfvén velocity is almost zero and the magnetosonic velocity ranges between 1000 to 2000 km/s.

the *Tsyganenko* [1989] provides average magnetic field values in the plasma sheet and may not be accurate at any particular instant in time. In particular, during substorms the plasma sheet goes through very dynamic changes, and its properties may not even be close to the average values predicted by the model.

Figure 10 shows the Alfvén (a) and the magnetosonic (b) velocity profiles in the meridian plane in OpenGGCM. The Alfvén and the magnetosonic velocities vary between 1500 and 4000 km/s in the lobes, and the magnetosonic velocity varies between 1000 and 1500 km/s in the plasma sheet. Comparing these velocities with the Figure 2 of *Lin et al.* [2009], the MHD wave velocity is much higher in the magnetotail of the OpenGGCM model.

In addition, *Lin et al.* [2009] assumed that waves propagate along plasma sheet field lines with the fast mode speed until $\sim -10\ R_E$ and then convert to Alfvén wave on closed field lines, which they called the Tamao's path. However, we find that the plasma sheet path is not generally the fastest path for waves originating in

the plasma sheet and that the waves travel faster through the lobes. As Figure 7 shows, signals travel faster to higher magnetic latitudes. Those waves did not arrive via the plasma sheet path. Instead, after being generated in the plasma sheet, they entered the lobes and traveled obliquely along lobe field lines directly to the ionosphere. *Uozumi et al.* [2000, 2004, 2007] also suggested that the signals arrive at higher latitudes tens of seconds earlier than the lower latitudes. This is also evident in Figure 2, which shows wave fronts in the lobes well ahead of the fronts following the plasma sheet path. Thus, even though the lobe path may be longer than the plasma sheet path, it is the faster path because the wave phase speed is several times faster in the lobes than in the plasma sheet.

5. Summary and Conclusions

The sequence of events leading to the onset of auroral substorm has been a long standing question in the field of magnetosphere physics. It is not clear what phenomenon triggers the onset of a substorm because most of the observed disturbances happen within minutes of auroral onset. Since the MHD waves carry energy through different regions of the magnetotail and eventually to the ionosphere, it is critically important to determine the MHD wave travel time in the magnetotail. Previously, two studies focused on wave travel time in the magnetotail, i.e., *Lin et al.* [2009] and *Chi et al.* [2009]. *Lin et al.* [2009] assumed that MHD waves propagate through the plasma sheet with fast mode speed and later convert to the Alfvén mode waves upon reaching the dipolar field of the Earth. Also, both studies used empirical models to calculate the wave velocities.

Here we used OpenGGCM model to investigate wave travel times and wave modes in the magnetotail. We launched waves by creating a single impulse or sinusoidal pulsations at different points in the plasma sheet and performed wave analysis to distinguish different modes of the MHD waves at various regions of the tail. Ground magnetic perturbation (ΔB_θ) and Δ FAC were used as indicators of wave arrival time in the ionosphere. By using the global MHD simulation model, we obtain more realistic results because the magnetosphere configuration is calculated self-consistently. The main outcomes of this study are as follows:

1. It takes approximately 70 s for a wave to travel from midtail region to the ionosphere. This travel time is faster than previously reported MHD wave travel times.
2. The wave paths are more complicated than the so-called Tamao path, and waves can take different paths to reach the ionosphere.
3. The fastest waves do not travel along the plasma sheet but have shorter travel times through the lobes.
4. The impulses that are generated closer to earth lead to latitudinally spread out ionosphere signatures, whereas the signals that originated in the midtail region lead to more localized signatures.
5. The waves travel as fast mode in the plasma sheet and the lobes of the midtail regions. However, they convert to Alfvén mode when they reach strong gradients in the magnetic field or in the density, for example, in the PSBL or near the Earth.
6. Based on the OpenGGCM signal arrival time, we find the average wave speeds to be around 3000 and 1700 km/s in the lobe and plasma sheet paths, respectively.

Acknowledgments
This work was supported by grant AGS-1143895 from the National Science Foundation and subcontract SA405826326 to UCB (NASA/THEMIS). Computations were performed on Trillian, a Cray XE6m-200 supercomputer at University of New Hampshire supported by the NSF MRI program under grant PHY-1229408. The simulation data used to produce the figures can be obtained from the authors upon request. Most of the plots were generated using visualizing package, Viscid, and we would like to thank Viscid's developer Kristofor Maynard.

References

Allan, W., and A. N. Wright (2000), Magnetotail waveguide: Fast and Alfvén waves in the plasma sheet boundary layer and lobe, *J. Geophys. Res.*, *105*(A1), 317–328.

Angelopoulos, V., et al. (2008), Tail reconnection triggering substorm onset, *Science*, *321*(5891), 931–935.

Baker, D. N., T. Pulkkinen, V. Angelopoulos, W. Baumjohann, and R. McPherron (1996), Neutral line model of substorms: Past results and present view, *J. Geophys. Res.*, *101*, 12–975.

Chi, P. J., and C. T. Russell (2005), Travel-time magnetoseismology: Magnetospheric sounding by timing the tremors in space, *Geophys. Res. Lett.*, *32*, L18108, doi:10.1029/2005GL023441.

Chi, P. J., C. T. Russell, J. Raeder, E. Zesta, K. Yumoto, H. Kawano, K. Kitamura, S. M Petrinec, V. Angelopoulos, G. Le, and M. B. Moldwin (2001), Propagation of the preliminary reverse impulse of sudden commencements to low latitudes, *J. Geophys. Res.*, *106*, 18,857–18,864.

Chi, P. J., D. H. Lee, and C. T. Russell (2006), Tamao travel time of sudden impulses and its relationship to ionospheric convection vortices, *J. Geophys. Res.*, *111*, A08205, doi:10.1029/2005JA011578.

Chi, P. J., C. Russell, and S. Ohtani (2009), Substorm onset timing via traveltime magnetoseismology, *Geophys. Res. Lett.*, *36*, L08107, doi:10.1029/2008GL036574.

Connor, H., J. Raeder, and K. Trattner (2012), Dynamic modeling of cusp ion structures, *J. Geophys. Res.*, *117*, A04203, doi:10.1029/2011JA017203.

Connor, H., E. Zesta, D. Ober, and J. Raeder (2014), The relation between transpolar potential and reconnection rates during sudden enhancement of solar wind dynamic pressure: OpenGGCM-CTIM results, *J. Geophys. Res. Space Physics*, *119*, 3411–3429, doi:10.1002/2013JA019728.

Connor, H., J. Raeder, D. Sibeck, and K. Trattner (2015), Relation between cusp ion structures and dayside reconnection for four imf clock angles: OpenGGCM-CTIM results, *J. Geophys. Res. Space Physics*, *120*, 4890–4906, doi:10.1002/2015JA021156.

Fedder, J., and J. Lyon (1987), The solar wind-magnetosphere-ionosphere current-voltage relationship, *Geophys. Res. Lett.*, *14*(8), 880–883.
Fuller-Rowell, T., D. Rees, S. Quegan, R. Moffett, and M. Codrescu (1996), A coupled thermosphere-ionosphere model (CTIM), *STEP Rep. 239*.
Gabrielse, C., et al. (2009), Timing and localization of near-Earth tail and ionospheric signatures during a substorm onset, *J. Geophys. Res.*, *114*, A00C13, doi:10.1029/2008JA013583.
Ge, Y., J. Raeder, V. Angelopoulos, M. Gilson, and A. Runov (2011), Interaction of dipolarization fronts within multiple bursty bulk flows in global MHD simulations of a substorm on 27 February 2009, *J. Geophys. Res.*, *116*, A00I23, doi:10.1029/2010JA015758.
Gilson, M., J. Raeder, E. Donovan, Y. Ge, and L. Kepko (2012), Global simulation of proton precipitation due to field line curvature during substorms, *J. Geophys. Res.*, *117*, A05216, doi:10.1029/2012JA017562.
Hones, E. W. (1984), Magnetic reconnection in space and laboratory plasmas, *Eos Trans. AGU*, *65*(18), 340–341.
Keiling, A., G. Parks, J. Wygant, J. Dombeck, F. Mozer, C. Russell, A. Streltsov, and W. Lotko (2005), Some properties of Alfvén waves: Observations in the tail lobes and the plasma sheet boundary layer, *J. Geophys. Res.*, *110*, A10S11, doi:10.1029/2004JA010907.
Kivelson, M. G., and C. T. Russell (1995), *Introduction to Space Physics*, Cambridge Univ. Press, Cambridge, U. K.
Lin, N., H. Frey, S. Mende, F. Mozer, R. Lysak, Y. Song, and V. Angelopoulos (2009), Statistical study of substorm timing sequence, *J. Geophys. Res.*, *114*, A12204, doi:10.1029/2009JA014381.
Liou, K., C. I. Meng, P. T. Newell, K. Takahashi, S. I. Ohtani, A. T. Y. Lui, M. Brittnacher, and G. Parks (2000), Evaluation of low-latitude Pi2 pulsations as indicators of substorm onset using Polar ultraviolet imagery, *J. Geophys. Res.*, *105*(A2), 2495–2505, doi:10.1029/1999JA900416.
Lui, A. (1996), Current disruption in the Earth's magnetosphere: Observations and models, *J. Geophys. Res.*, *101*(A6), 13,067–13,088.
Lui, A. (2004), Potential plasma instabilities for substorm expansion onsets, *Space Sci. Rev.*, *113*(1–2), 127–206.
Lui, A. (2009), Comment on tail reconnection triggering substorm onset, *Science*, *324*(5933), 1391–1391.
Lyons, L., Y. Nishimura, Y. Shi, S. Zou, H.-J. Kim, V. Angelopoulos, C. Heinselman, M. Nicolls, and K.-H. Fornacon (2010), Substorm triggering by new plasma intrusion: Incoherent-scatter radar observations, *J. Geophys. Res.*, *115*, A07223, doi:10.1029/2009JA015168.
Lysak, R., Y. Song, M. Sciffer, and C. Waters (2015), Propagation of Pi2 pulsations in a dipole model of the magnetosphere, *J. Geophys. Res. Space Physics*, *120*, 355–367, doi:10.1002/2014JA020625.
Lysak, R. L., and Y. Song (2004), Propagation of Alfvén waves at the plasma sheet boundary layer, in *Proceedings of the 7th International Conference on Substorms*, edited by T. Pulkinnen and N. Ganushkina, p. 81, FMI Publ., Finnish Meteorological Institute, Helsinki.
Nishimura, Y., L. Lyons, S. Zou, V. Angelopoulos, and S. Mende (2010), Substorm triggering by new plasma intrusion: THEMIS all-sky imager observations, *J. Geophys. Res.*, *115*, A07222, doi:10.1029/2009JA015166.
Oliveira, D. M., and J. Raeder (2014), Impact angle control of interplanetary shock geoeffectiveness, *J. Geophys. Res. Space Physics*, *119*, 8188–8201, doi:10.1002/2014JA020275.
Priest, E. R. (2012), Solar magnetohydrodynamics, *Springer*, *21*.
Raeder, J. (2003), Global geospace modeling: Tutorial and review, in *Space Plasma Simulation*, vol. 615, p. 84, Springer, Heidelberg, Germany.
Raeder, J. (2006), *Flux transfer events: 1. Generation mechanism for strong southward IMF*, 381–392, vol. 24.
Raeder, J., R. McPherron, L. Frank, S. Kokubun, G. Lu, T. Mukai, W. Paterson, J. Sigwarth, H. Singer, and J. Slavin (2001a), Global simulation of the geospace environment modeling substorm challenge event, *J. Geophys. Res.*, *106*(A1), 381–395.
Raeder, J., Y. Wang, and T. J. Fuller-Rowell (2001b), Geomagnetic storm simulation with a coupled magnetosphere-ionosphere-thermosphere model, in *Space Weather: Progress and Challenges in Research and Applications, Geophys. Monogr.*, vol. 125, edited by P. Song, H. J. Singer, and G. Siscoe, pp. 377–384, AGU, Washington, D. C.
Raeder, J., D. Larson, W. Li, E. L. Kepko, and T. Fuller-Rowell (2009), Openggcm simulations for the themis mission, *Space Sci. Rev.*, *141*, 535–555.
Raeder, J., P. Zhu, Y. Ge, and G. Siscoe (2010), Open Geospace General Circulation Model simulation of a substorm: Axial tail instability andballooning mode preceding substorm onset, *J. Geophys. Res.*, *115*, A00I16, doi:10.1029/2010JA015876.
Raeder, J., P. Zhu, Y. Ge, and G. Siscoe (2013), Auroral signatures of ballooning mode near substorm onset: OpenGGCM simulations, in *Auroral Phenomenology and Magnetospheric Processes: Earth And Other Planets*, vol. 197, edited by A. Keiling et al., pp. 389–396, AGU, Washington, D. C.
Roux, A., S. Perraut, P. Robert, A. Morane, A. Pedersen, A. Korth, G. Kremser, B. Aparicio, D. Rodgers, and R. Pellinen (1991), Plasma sheet instability related to the westward traveling surge, *J. Geophys. Res.*, *96*(A10), 17,697–17,714.
Russell, C., and R. McPherron (1973), The magnetotail and substorms, *Space Sci. Rev.*, *15*(2–3), 205–266.
Tamao, T. (1964), The structure of three-dimensional hydromagnetic waves in a uniform cold plasma, *J. Geomagn. Geoelectr.*, *16*(2), 89–114.
Tsyganenko, N. (1989), A magnetospheric magnetic field model with a warped tail current sheet, *Planet. Space Sci.*, *37*(1), 5–20.
Uozumi, T., K. Yumoto, H. Kawano, A. Yoshikawa, J. Olson, S.-I. Akasofu, and E. Vershinin (2000), Propagation Characteristics of energy transfer of Pi 2 magnetic pulsations: Latitudinal dependence, *Geophys. Res. Lett.*, *27*(11), 1619–1622.
Uozumi, T., et al. (2004), Propagation characteristics of Pi2 magnetic pulsations observed at ground high latitudes, *J. Geophys. Res.*, *109*, A08203, doi:10.1029/2003JA009898.
Uozumi, T., H. Kawano, A. Yoshikawa, M. Itonaga, and K. Yumoto (2007), Pi2 source region in the magnetosphere deduced from CPMN data, *Planet. Space Sci.*, *55*(6), 849–857, doi:10.1016/j.pss.2006.03.016.
Zhu, P., J. Raeder, K. Germaschewski, and C. C. Hegna (2009), Initiation of ballooning instability in the near-Earth plasma sheet prior to the 23 March 2007 THEMIS substorm expansion onset, *Ann. Geophys.*, *27*, 1129–1138.